Measurement 123 (2018) 163–174

Contents lists available at ScienceDirect

Measurement

journal homepage: www.elsevier.com/locate/measurement

A new measurement system using magnetic flux leakage method in pipeline inspection

Yavuz Ege*, Mustafa Coramik

Balikesir University, Necatibey Faculty of Education, Department of Physics, 10100 Balikesir, Turkey

ARTICLE INFO

Keywords:
AMR sensors
Crack
Data acquisition
LabVIEW
Magnetic flux leakage
Non-destructive testing
Pipelines

ABSTRACT

Today, natural gas and oil, called main energy sources, are transported by pipelines at long distances. Defects (corrosion, cracks, dents) in the buried pipelines can cause loss of life, environmental pollution and economic loss. Recently, devices called "Pipeline Inspection Gauge (PIG)" are used for non-destructive evaluation (NDE) of defects in pipelines. In these devices, the magnetic flux leakage (MFL) technique comes into prominence as the inspection method. However, when the literature is examined, a study that examines the speed variable for defect detection has not been found. In this study, two new PIGs which can be used to investigate the speed variable while determining defects in pipelines are designed. For these new designs, a new magnetic measurement system with KMZ51 AMR sensors is developed. The voltage values of the sensors in the measurement system are saved to the computer by using LabVIEW-based software in sequential order via the NI USB-6210 data acquisition card. This data is also displayed on LCD screens by using MyRIO 1900. In the article, the mechanics of the developed system, its electronics and its software are examined in detail. Moreover, the usability of these new designs in determining pipeline defects are examined through an example experiment result with the Origin analysis program.

1. Introduction

Pipelines are widely used to transport natural gas and petroleum products between countries or at long distances [1,2]. In most of these buried pipelines, external factors such as corrosion pressure or displacement can cause defects [3]. These defects can result in economic losses, environmental pollution and fatal accidents if they are not detected on time. It is necessary to inspect the pipelines regularly in order to avoid these problems [4].

Devices called "Pipeline Inspection Gauge (PIG)", designed in accordance with non-destructive testing (NDE) techniques, can perform the inspection without damaging the pipeline. Only one or few of the several different techniques can be used together in the design of the PIGs that are used in the pipeline inspection. These techniques are mainly ultrasonic [5,6], magnetic flux leakage [7–10] and eddy currents [11]. Also metal magnetic memory [12–14], magnetic Barkhausen noise [15,16], magneto acoustic emission [17] and magnetic tomography [18] methods are used for defect detection. Among these techniques, which have advantages and disadvantages relative to each other, the magnetic flux leakage method (MFL) has been considerably used in the design of PIG in recent years. This method, which is used in the inspection of ferromagnetic materials, focuses on the detection of defects on the magnetized sample by detecting magnetic anomalies in magnetic flux lines with using magnetic sensors. Parallel to the developments in magnetic sensor technology, the types of sensors used in the magnetic flux leakage technique is also considerably increased. In recent years, the crack detection studies which uses the MFL method have frequently used Giant Magneto Resistive (GMR) [19], Anisotropic Magneto Resistive (AMR) [7], Giant Magneto Impedance (GMI) [20] and Magneto Optical (MO) [21] sensors as well as Hall sensors [22,23] and search coils [24].

In the magnetic flux leakage technique, magnets or coils are used to magnetize the samples. Two different magnetization types are used in this PIGs; circumferential magnetization and axial magnetization. Axial MFL devices that axially magnetize the pipe sample are used to determine circumferential defects. Circumferential MFL (CMFL) devices which circumferentially magnetize the sample are used in determining axial defects [25,26]. Also the usage of Pulsed Magnetic Field Leakage (PMFL) technique is increasing last years [19]. With pulsed MFL, the probe is driven with a square waveform and the frequency components can provide information from different depths [27]. Also, PMFL technique is used for measuring stress in ferromagnetic metals [28].

When the studies that use the MFL method are reviewed in the literature, it is seen that they are generally focused on different sensor

* Corresponding author.
E-mail addresses: yavuzege@gmail.com (Y. Ege), mustafacoramik@balikesir.edu.tr (M. Coramik).

https://doi.org/10.1016/j.measurement.2018.03.064
Received 16 November 2017; Received in revised form 26 March 2018; Accepted 27 March 2018
Available online 28 March 2018

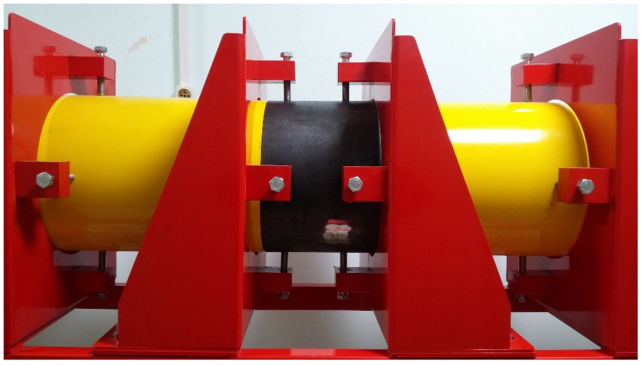

Fig. 1. View of defective pipe.

Fig. 2. General view of the system.

usage. No study has been found to examine the change in magnetic sensor output voltages for PIGs with different speeds. For this purpose, two different PIGs are developed in this study and they can magnetize the pipeline axially and circumferentially. KMZ 51 AMR sensors are installed on the developed PIGs. In addition, coils with iron-carbon alloy cores containing more than 2% carbon are used to magnetize the pipe sample. The movement of the PIG in the pipe is provided by a three-phase AC motor with a trigger belt. The AC motor is driven by a frequency inverter (speed controller) so that the speed of the PIG is changed.

The developed PIGs are moved in the steel pipes, produced as High Frequency Welding with a length of 5.25 m. The defected pipe is placed in the middle of the movement area (Fig. 1).

Table 1
Technical data of motor and reductor.

Motor						
Full Load					Starting	
Power (kW)	Rev. per minute (rpm)	Current (A)	Moment (N m)	Power Factor (cos φ)	Current (I/INA)	Moment (MA/MN)
1.50	1440	3.40	9.95	0.77	6.00	2.30
Reductor						
Power (kW)				Revolutions per minute (rpm)		
1.50				106		

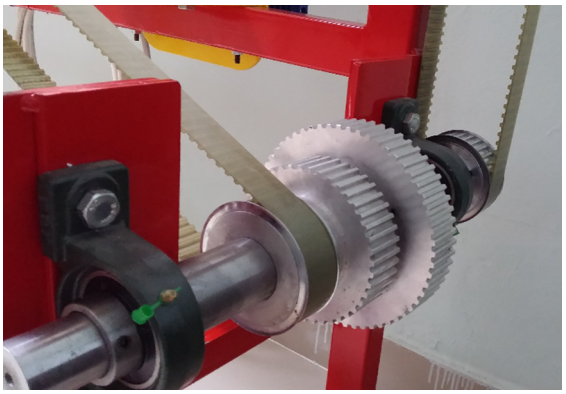

Fig. 4. Timing belts, gears and ball bearing units.

The programs, which are written by using the LabVIEW programming language, are used to save the data to the computer and display them on the control panel. The NI USB-6210 data acquisition card and My-RIO 1900 card are also used in the system. In other parts of the manuscript, the PIGs and the components and the design of the developed system are explained in detail.

2. Components and design of the system

A general view of the measuring system, developed within the scope of the study and used for identifying the defects in pipelines at different speeds, is given in Fig. 2. The developed system consists of three parts as mechanical, electronic and software. The sub-systems of the

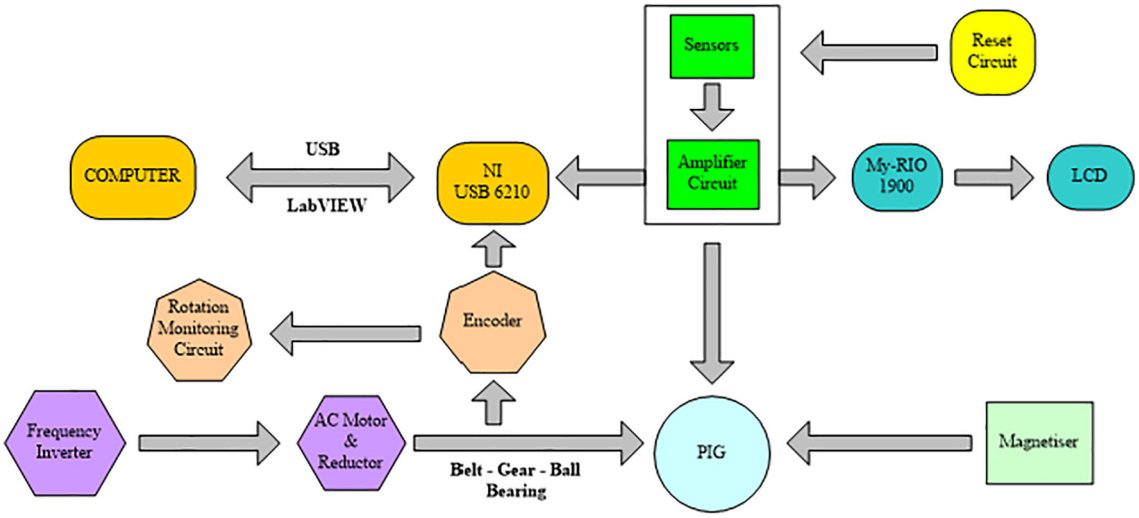

Fig. 3. Schematic representation of system components interactions with each other.

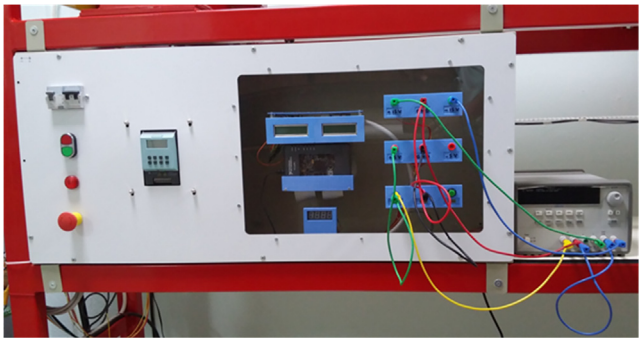

Fig. 5. View of the control panel.

measurement system and their interactions with each other are given in the schematic representation in Fig. 3.

In the study, firstly the mechanical system is designed and manufactured, then the electronic system is installed into this system. Finally the data is saved and displayed on a computer with LabVIEW-based program.

2.1. Mechanical system

The mechanical system consists of the structure on which defects and non-defective pipe samples are placed, eight fixing plates and three phase AC motor and reductor, timing belts, gears and ball bearing units, providing for the movement of the PIGs.

The structure with dimensions of 174 cm × 540 cm, which is the carrier of the system, is produced by iron profile with the dimensions of 40 mm × 40 mm and 40 mm × 60 mm. The fixing plates are designed to ensure the pipes, to be used in the experiments, immobilized in the system (Fig. 2).

The three phase AC motor and the reductor connected to it are the parts that provide the movement in the system. Technical data of the motor and the reductor are given in Table 1.

Three T10 type polyurethane steel cord timing belts and 12 aluminium gears are used as transmission elements in the system. One of the belts with 10 mm pitch and 32 mm width is open end and the other two are endless. 12 ball bearing units are also used for motion transmission in the mechanical system (Fig. 4).

2.2. Electronic system

The electronic system includes PIGs, frequency inverter (speed controller), magnetic sensors, amplifier circuits, reset circuit for the magnetic sensor, the NI-USB 6210 data acquisition card, the NI-MyRIO-1900, encoder, rotation monitoring circuit and LCDs.

Connection cables of the electronic system components are collected in the control panel. In addition, the inputs of the supply voltages, required for the system, are located at the right side of the control panel.

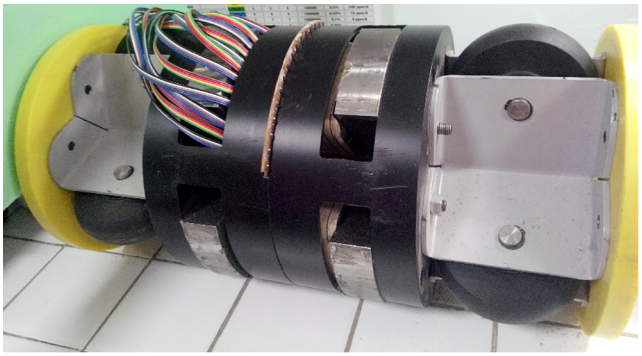

Fig. 7. Produced axial PIG.

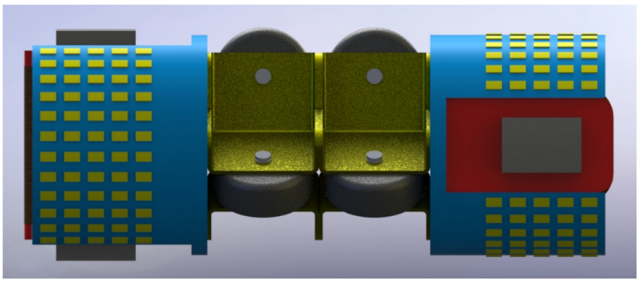

Fig. 8. Design of circumferential PIG.

Fig. 9. Produced circumferential PIG.

The connection between the power supply and the electronic system is provided by these inputs (Fig. 5).

2.2.1. PIGs

Two different PIGs are designed for collecting data from the pipeline. The movement of the PIGs in the pipe is provided by the timing belts fixed to the PIGs from both sides.

The first designed PIG aims to determine the circumferential defects in the pipeline. The first PIG, called Axial PIG, consists of magnetic sensors, signal amplification circuits, 4 coils with iron-carbon alloy core (more than 2% carbon ratio) and 6 wheels. PIG is produced by using

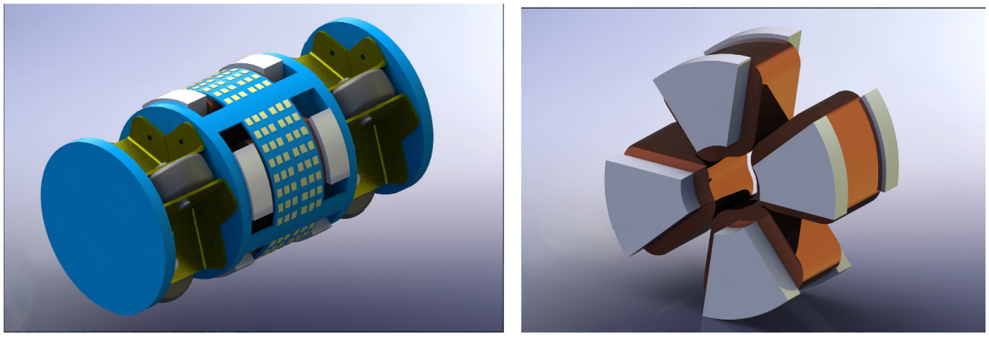

Fig. 6. Design of axial PIG and coils with core.

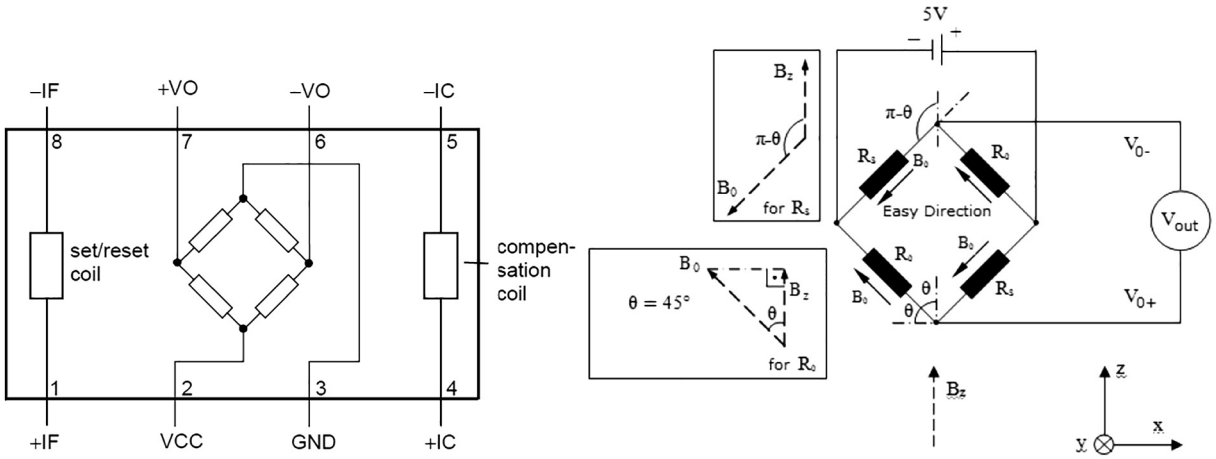

Fig. 10. (a) Block structure of KMZ51 AMR sensor, (b) The circuit diagram of the KMZ51 AMR sensor.

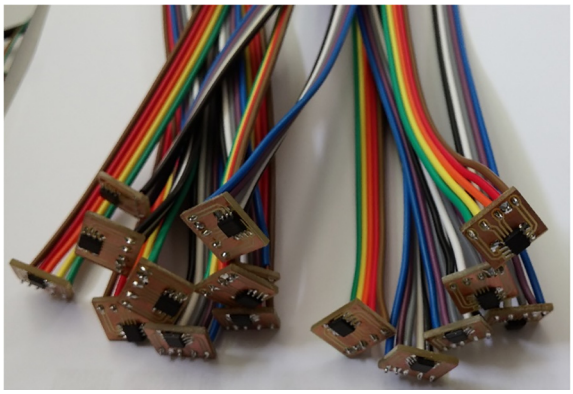

Fig. 11. Printed circuit boards of the KMZ 51.

non-magnetic castermid and aluminium materials. The technical drawings of the axial PIG and the core coil at the design phase are given in Fig. 6.

The iron-carbon alloy core in the PIG is geometrically designed to axially magnetize the pipe homogeneously. A copper wire with a diameter of 1 mm is wrapped around the cores and the coils with 1200 springs are produced. The axial PIG on which the magnetic sensors and signal amplifier circuits are mounted is given in Fig. 7.

The connections between the PIG and the NI-USB 6210 are made by ribbon cables. The coils of the cores are powered by 0.75 mm diameter copper cables located on the opposite side of the ribbon cable.

The second PIG is designed to detect axial defects in the pipeline (Fig. 8).

In this PIG, the pipeline is magnetized circumferentially to determine axial defects in the pipeline. For this purpose, two rectangular prism-shaped cores which are positioned perpendicular to each other and whose ends have a suitable geometry with the inner surface of the pipe are used. By this way, the defects that can be caught under the first core during the movement of the PIG can be detected by the magnetic sensors around the second core. 1000 turns are made on each iron-carbon alloy core using 1 mm diameter copper wire. In the circumferential PIG, the power lines of the coil and data acquisition lines are positioned opposite. Six castermid wheels are used for the movement of the PIG in the pipeline. Other components on the PIG are also made from castermid and aluminium. The photograph of the finished circumferential PIG is given in Fig. 9.

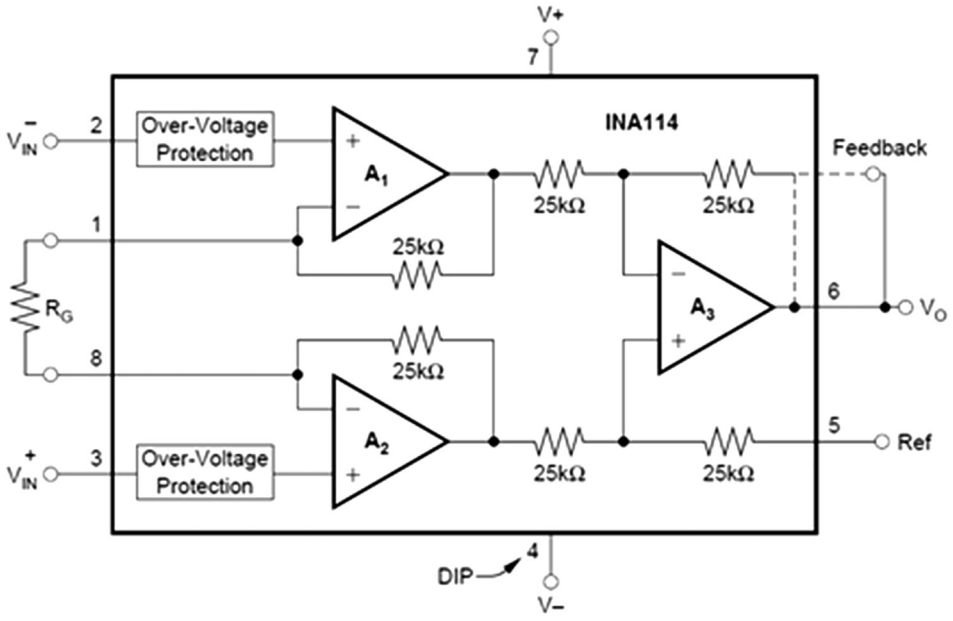

Fig. 12. Block structure of INA114.

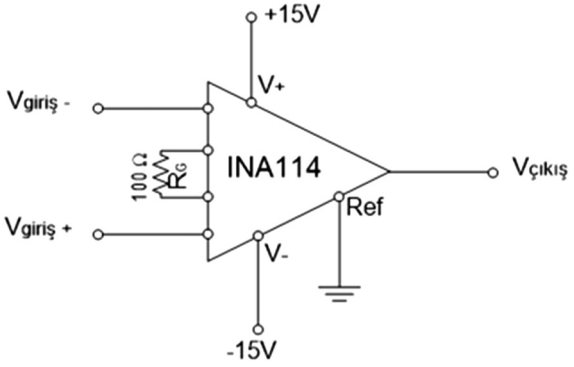

Fig. 13. Schematic of amplifier circuit.

2.2.2. Magnetic sensors

In the magnetic measurement system, KMZ51 AMR sensors manufactured by Philips are used. These sensors, which can measure with high precision, internally include compensation coil and flip coil. The KMZ51 has high sensitivity in detecting magnetic fields, a wide operating temperature range and low sensitivity to mechanical pressures. It is composed of four thin films connected as a Wheatstone bridge. If there is no magnetic field (B_z), then the outputs, V0 + and V0 − give the same values. However, in the case of magnetic field (B_z), the value of the resistances of the thin films change and a potential difference occurs between V0 + and V0 −. The KMZ 51 has many applications such as compass, navigation, metal detection and traffic control [29–32].

The block structure of the KMZ 51 sensor and the circuit diagram of the sensor are shown in Fig. 10a, b.

The sensitivity of the KMZ51 sensor, which can be supplied with a voltage between 5 V and 8 V, is 16 (mV/V)/(kA/m). The printed circuit boards of the KMZ 51 sensors are shown in Fig. 11.

2.2.3. Frequency inverter (speed controller)

Siemens Sinamics G110 (speed controller) is used for the purpose of setting the input frequency of the three-phase AC motor which determines the speed of the PIG in the system. The programmable device allows the frequency of the grid voltage to be changed. By changing the input frequency of the AC motor, the speed of the PIG connected to the timing belt and the speed of the AC motor can be adjusted. The output frequency range of the speed controller is 0–650 Hz and the input frequency range of the speed controller is 47–63 Hz. The device's frequency setting and direction setting buttons are located on the control panel.

2.2.4. Amplifier circuit

An amplifier circuit is designed to amplify the output signals of the magnetic sensors by using INA114. The INA114 is a low cost, general purpose instrumentation amplifier offering excellent accuracy. The INA114, consisting of three opamp circuits, can amplify signals between 1 and 10,000 times by using a single external resistor (Fig. 12).

The gain formula for INA114 is given in Eq. (1).

$$G = 1 + \frac{50\ \text{k}\Omega}{R_C} \tag{1}$$

The sensor output signals are increased 501 times in the developed amplifier circuit by using the RG = 100 Ω resistor between pins 1 and 8 of INA114. Also, each reference pin of the INA114 is grounded

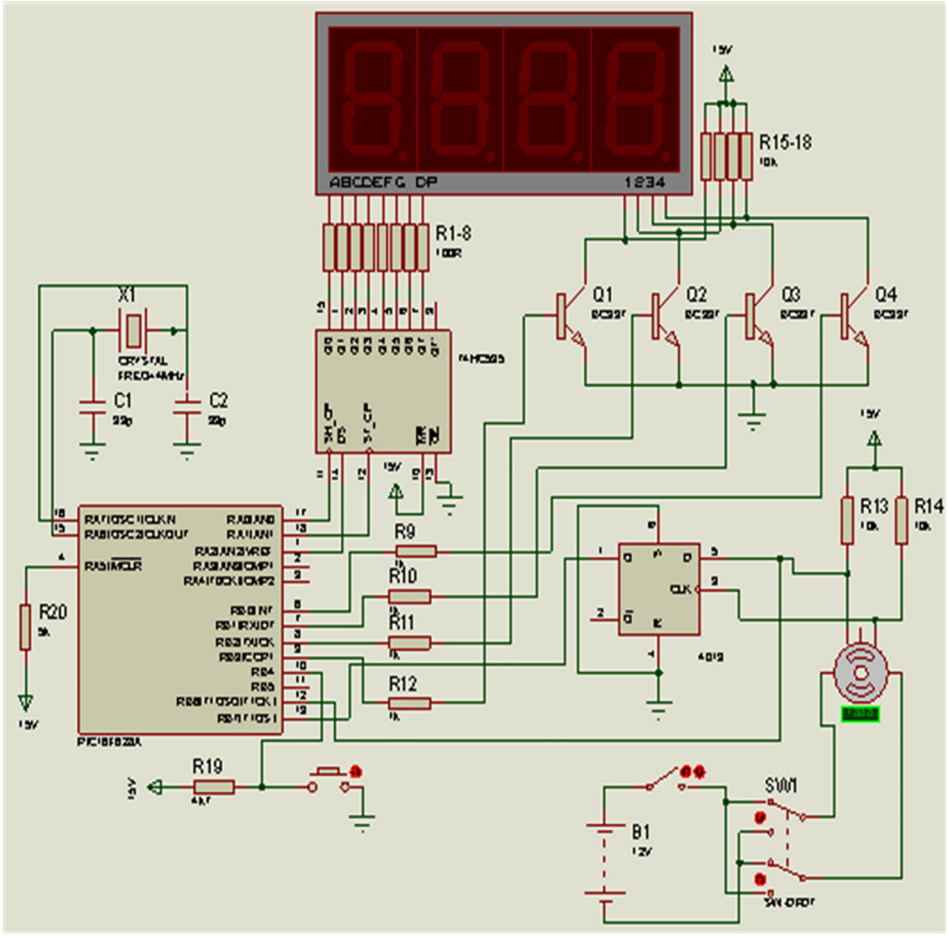

Fig. 14. Circuit diagram of rotation monitoring circuit.

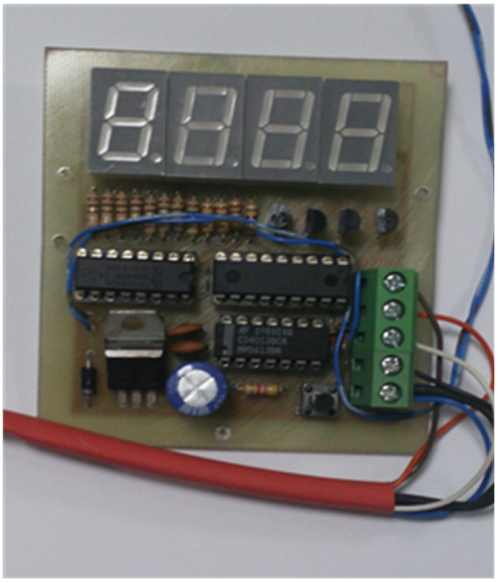

Fig. 15. Rotation monitoring circuit.

(Fig. 13). Printed circuit boards, which have 16 amplifier circuits, are manufactured for each PIG and mounted on them.

2.2.5. Encoder and rotation monitoring circuit

The encoder is mounted on one of the shafts so that the movement of the PIG can be monitored from the control panel of the system. In addition, a circuit is developed which shows the angle of rotation of the encoder. The encoder with a 5–24 V DC supply voltage range produces 1024 pulses per tour. According to the number of pulses, the rotation angle of the shaft is displayed on the screen. The circuit diagram of the rotation monitoring circuit, which shows the rotation angle of the shaft, is given in Fig. 14.

In the circuit, PIC 16F628A microcontroller, 74HC595 shift-register integrated circuit and CD4013 flip-flop integrated circuit are used (Fig. 15). The program embedded in the microcontroller is written by using the C programming language.

2.2.6. Data monitoring screen

A data monitoring screen is created to view the output voltages of the sensors instantly by using two Pmod CLS LCD, an NI MyRIO-1900 and a multiplexer (Fig. 16).

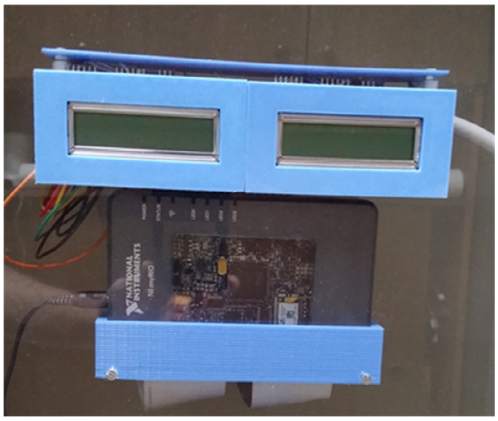

Fig. 16. Data monitoring screen.

The NI MyRIO-1900 is a portable and programmable device that can be used in systems such as control, robotics, and mechatronics. The NI MyRio-1900, which has analog inputs (AI), analog outputs (AO), digital inputs and outputs (DIO), power output, and audio input and output channels, can be connected to the computer via USB or wireless. There are 8 analog input channels in 0–5 V range and 2 analog input channels in ± 10 V range (12 bit, 500 kS/s). In addition, there are 4 analog channels with output voltage in 0–5 V range and 2 analog channels with output voltage in ± 10 V range (12 bit, 345 kS/s). The number of channels that can be used as digital input and output is 40. The device has a Xilinx Z-7010 processor and has +3.3 V, +5.0 V, +15.0 V and −15.0 V terminals.

The Pmod CLS LCD, which is used in the circuit, has an Atmel ATmega48 microprocessor and it has a 16 × 2 character display area. The 16-channel analog multiplexer allows to switch between the desired channel and the SIG channel according to the logic values entered at the S0, S1, S2 and S3 terminals.

Voltage values collected with the NI MyRIO-1900 are transferred to the LCD screen by using the UART protocol. The developed LabVIEW-based software is embedded into MyRIO to operate as stand-alone for switching the multiplexer and operating the UART protocol. A protection circuit has been developed so that if the output voltages of the sensors are greater than 10 V, the voltage will not damage My-RIO. The circuit diagram of the data monitoring screen is given in Fig. 17.

2.2.7. NI USB-6210

The voltage values obtained from the magnetic sensors are transferred to the computer environment via the NI USB-6210 data acquisition card after amplification. The USB-6210 multifunction DAQ has 16 analog inputs (16 bit, 250 kS/s), 4 digital inputs and 4 digital outputs. In addition, the device has two 32 bit counters. The device has a maximum analog input range of ± 10 V and has 91.6 μV sensitivity in this range.

2.2.8. Reset pulse circuit for magnetic sensors

If the KMZ51 AMR sensor saturates under strong magnetic field effect, the output voltages of the sensors do not change and remain at a constant value. In order to overcome this situation, a sensor reset pulse circuit is designed and the -If pins of the sensors are triggered briefly (Fig. 18). During the triggering, approximately 1 A current flows through the flip coils of the sensors and the sensors are out of saturation.

2.2.9. Power line

A power line consisting of a variac and a rectifier circuit is developed to supply current to the magnetizing coils located on the PIGs (Fig. 19). Four bridge diodes and eight 25 W 10 Ω resistors are used in the rectifier circuit.

2.3. Software

Two LabVIEW-based programs are written for recording and displaying the voltage values of the sensors. These programs are called data monitoring program and data recording program.

2.3.1. Data monitoring program

The data monitoring program is written with the purpose of displaying the sensor voltage values on the LCD in the control panel. State machine main structure is used in the program. The voltage values of the 8 sensors are updated on the display in approximately 50 ms intervals. The flow diagram of the program is given in Fig. 20.

In MyRIO-1900, the analog input is limited by two channels. For this reason, the sensor voltage values are sequentially displayed on the LCD by using a multiplexer. The multiplexer's S0, S1, S2 and S3

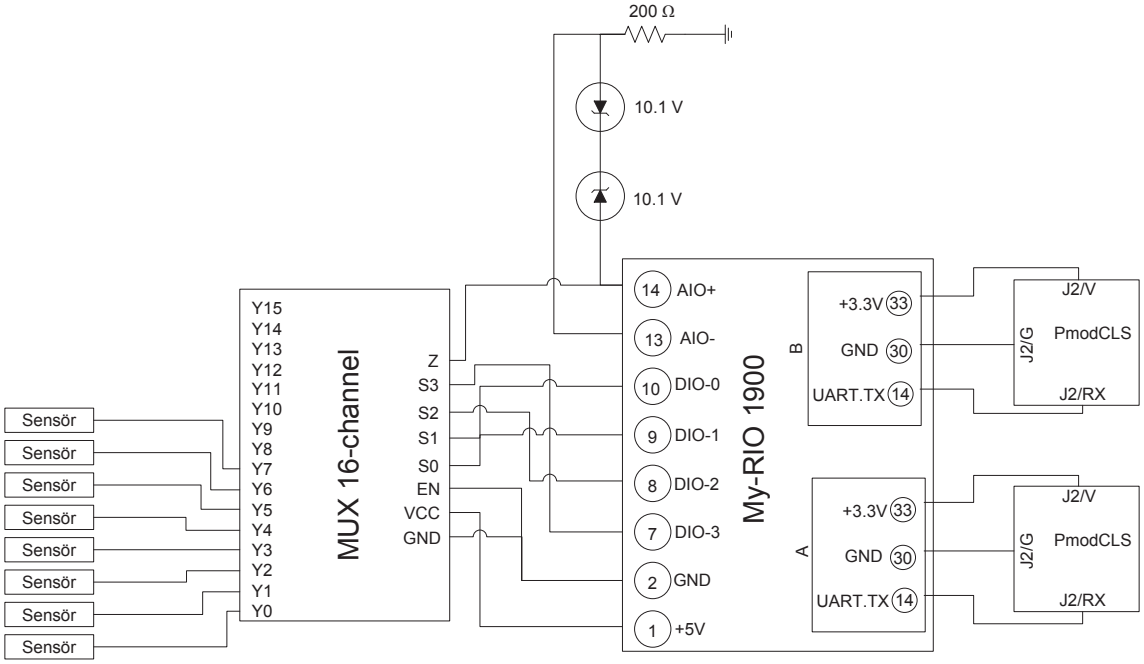

Fig. 17. Circuit diagram of the data monitoring screen.

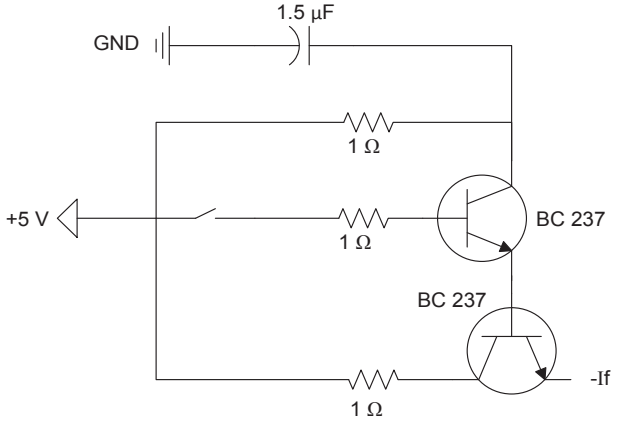

Fig. 18. Reset circuit.

terminals are triggered by My-RIO according to the truth table. Thus, each sensor is connected respectively to the Z channel, which is the common channel of the multiplexer. The sensor voltage values that stored in the memory by using the shift-register structure are displayed on the Pmod CLS LCD by using the UART protocol (Appendix A).

2.3.2. Data recording program

The data recording program is written for recording the sensor voltage values to the computer by using the trigger signals from the encoder. The flow diagram of the program is given in Fig. 21. When the speed is changed by using the frequency inverter (speed controller) on the control panel, the frequency of the pulses generated by the encoder changes. Depending on this change, the USB-6210 data acquisition card is triggered at different frequencies and the sensor voltage values are saved in a file with the extension xls. The block diagram structure of the data recording program is given in Appendix B.

3. Conclusion and discussion

In this study, two different PIGs which use the flux leakage method in the inspection of pipelines are designed and produced. In addition, a new magnetic measurement system is developed to investigate the effect of the speed variation of the produced PIGS to detect defects. In previous studies;

1. The effect of the PIG's speed in the pipeline was not investigated,
2. The KMZ AMR sensor was not used in the non-destructive evaluation of the pipelines,
3. Magnetic sensors mounted on the PIG were not replaced with different types (brand) of sensors,

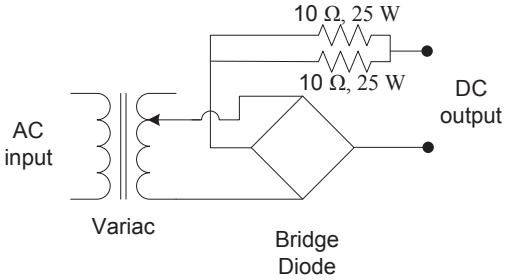

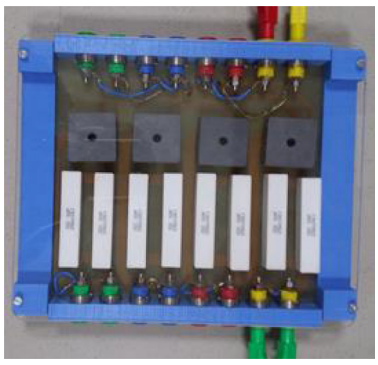

Fig. 19. Circuit diagram of rectifier circuit.

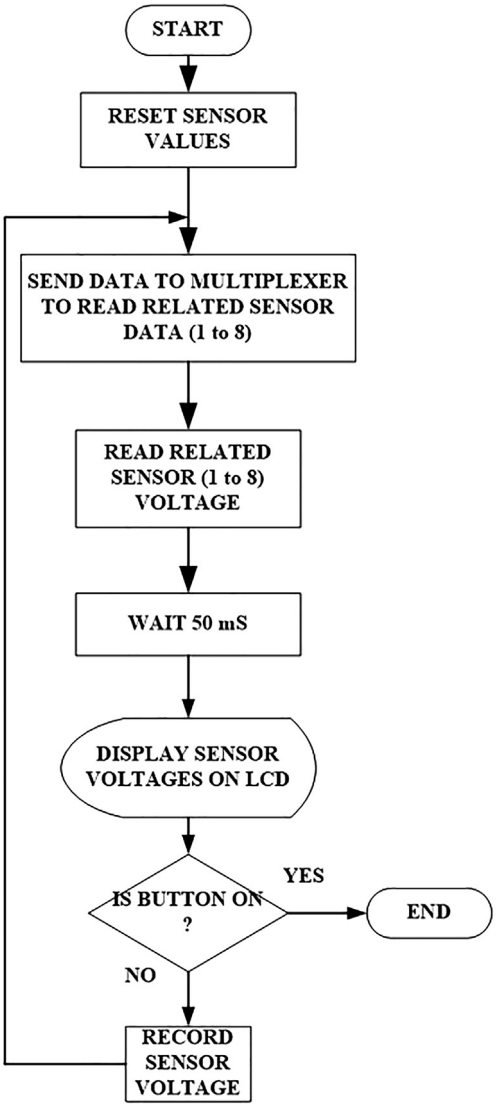

Fig. 20. Flow diagram of the data monitoring program.

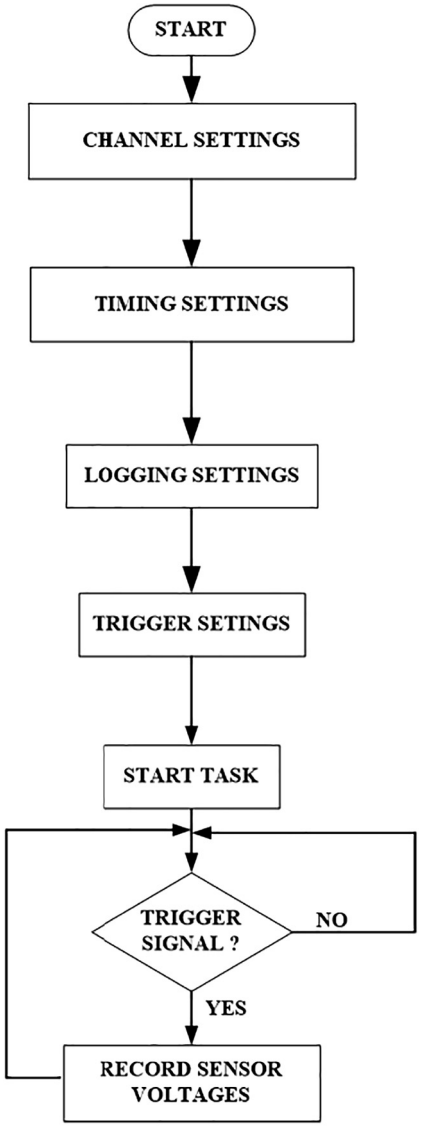

Fig. 21. Flow diagram of the data recording program.

4. Permanent magnets with constant magnetic field were used as magnetizing source in the magnetization of the pipe.
5. The world's magnetic field was not used for energy efficiency in the non-destructive evaluation of the pipelines.

These deficiencies are eliminated by the measurement system developed within the scope of the study.

The aim of this article is to explain the developed system in detail. The experimental results obtained from the system for different PIG velocities and different AC or DC magnetic field values are planned to be given in another manuscript. However, in this manuscript, an exemplary experimental results are given to demonstrate the usability of the system in the inspection of pipelines and its sensitivity of determining the defect.

In the example experiments, two artificial circumferential cracks are positioned on test pipeline with a 25 cm distance. Width of the first crack is 1 mm and the second crack is 2 mm. Two of the cracks are open to the outer surface. The sensor voltage values obtained on the inner side of the pipes according to the change in the horizontal component of the earth's magnetic field are recorded by the magnetic measurement

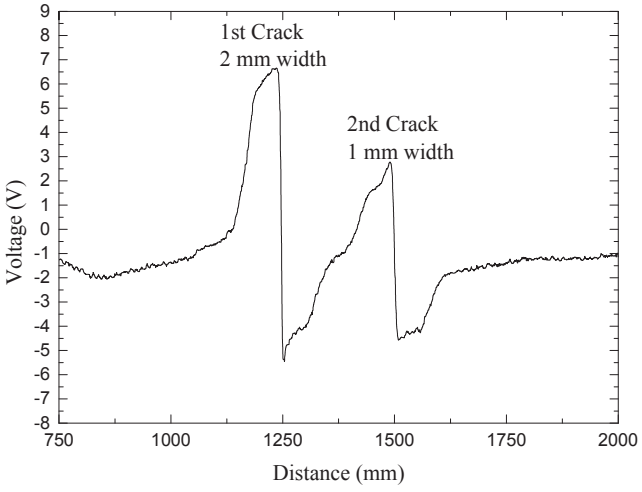

Fig. 22. 20 pts PF filtered sensor output voltages for 7.28 cm/s.

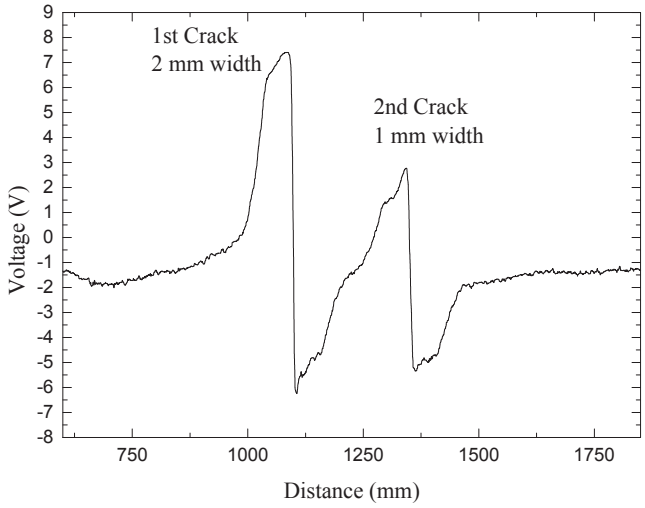

Fig. 23. 20 pts PF filtered sensor output voltages for 13.32 cm/s.

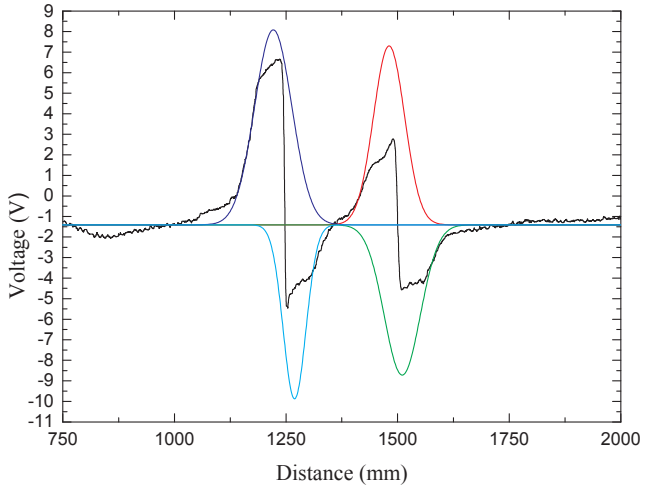

Fig. 24. 20 pts PF filtered multiple peak fit applied sensor output voltages for 7.28 cm/s.

system at different speeds of the PIG. The recorded data is noisy so it is filtered by the PF filter with the Origin analysis program. PF filter performs smoothing to noisy data. Point of window of the PF filter is selected 20 and percentile of the filter is selected 50. Then multiple peak fit is applied to the filtered data. The 20 pts PF filtered sensor output voltages for the different speed values are given at Figs. 22 and

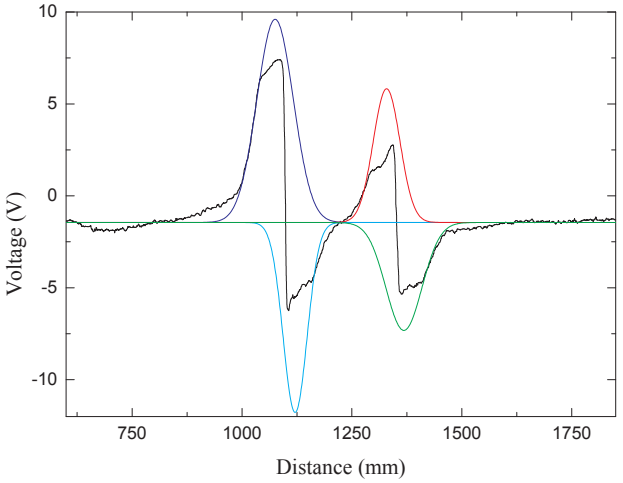

Fig. 25. 20 pts PF filtered multiple peak fit applied sensor output voltages for 13.32 cm/s.

23. When Figs. 22 and 23 are examined, it is seen that there is a change in the horizontal component of the Earth's magnetic field in the crack regions, and the sensor can detect it. The distance between positive peaks values of the filtered data are 253,713 mm and 257,644 mm, respectively. Also they are nearly the value of the distance between the artificial circumferential cracks.

Multiple peak fit applied data is given at Figs. 24 and 25.

When the Figs. 24 and 25 are examined, it is seen that the voltage signal consists of 4 gauss curves .The distance between the values of the 1st peak centre (blue[1]) and 3rd (red) peak centre of the gauss curves at x axis are 259,420 mm and 253,578 mm, respectively.

The Earth's magnetic field is about 10^{-5} Tesla and KMZ 51 sensors are also used in literature to determine the shape of magnetic materials by using earth's magnetic field [31,32]. Considering this situation, it can be said that the developed magnetic measuring system has high sensitivity in determining defects.

In addition to this, the fact that the researchers working in this area use a combination of different methods (such as Ultrasonic and MFL) can gain a different perspective on determining defects. Moreover, the position of the magnetic sensors on the PIG plays an important role in the MFL method due to the geometry of the defect in the pipe. Therefore, by using magnetic simulation programs such as Maxwell, different studies can be carried out about in which position the sensors will perform better.

Acknowledgements

This work was supported by the Balıkesir University Scientific Research Projects (BAP) (Project Number: 2.2014.0006).

[1] For interpretation of color in Figs. 24 and 25, the reader is referred to the web version of this article.

Appendix A

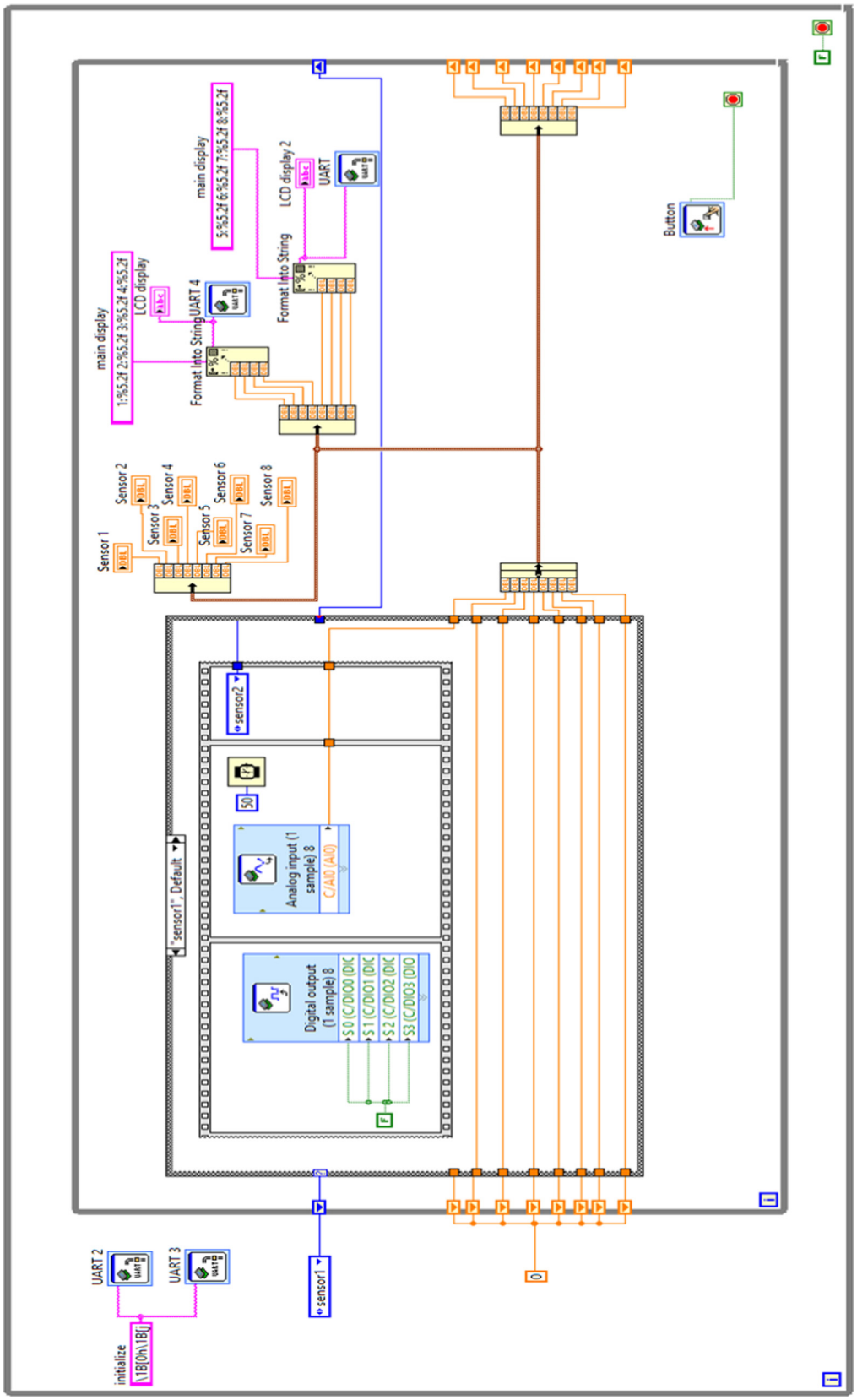
main display
1:%5.2f 2:%5.2f 3:%5.2f 4:%5.2f
LCD display
Format Into String
UART 4
main display
5:%5.2f 6:%5.2f 7:%5.2f 8:%5.2f
LCD display 2
Format Into String
UART
Button
Sensor 1
Sensor 2
Sensor 3
Sensor 4
Sensor 5
Sensor 6
Sensor 7
Sensor 8
sensor2
50
Analog input (1 sample) 8
C/AI0 (AI0)
"sensor1", Default
Digital output (1 sample) 8
S0 (C/DIO0) (DIC
S1 (C/DIO1) (DIC
S2 (C/DIO2) (DIC
S3 (C/DIO3) (DIO
0
sensor1
UART 2
UART 3
initialize
\1B[0h\1B[j

Appendix B

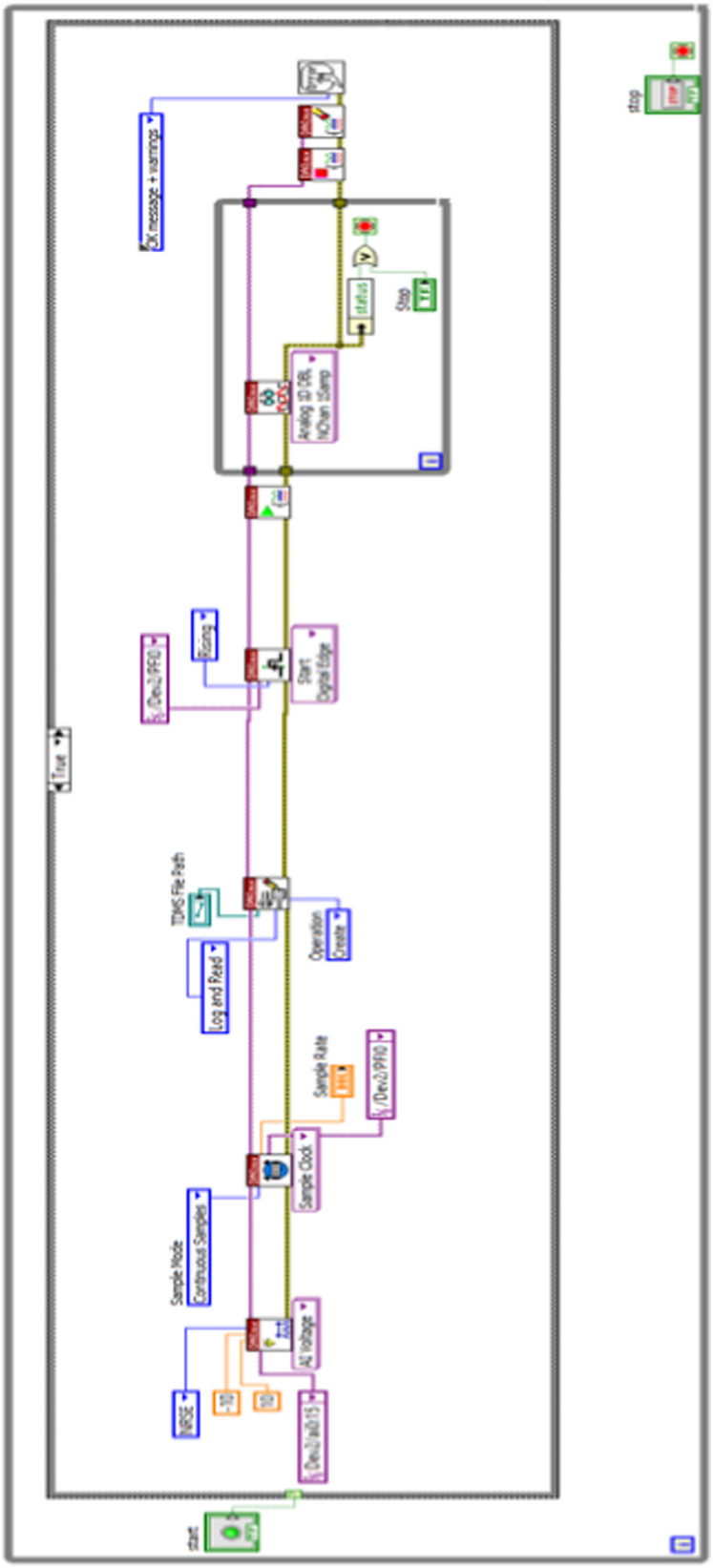
stop
OK message + warnings
Stop
Analog 1D DBL
nChan nSamp
Rising
Start
Digital Edge
True
TDMS File Path
Log and Read
Operation
Create
Sample Rate
Sample Clock
Sample Mode
Continuous Samples
AI Voltage
NRSE
start

References

[1] P.K. Nimje, C. Kannan, Q.M. Amir, Finite element modelling & experimental simulation of magnetic leakage flux from metal loss defects in steel pipelines, < http://www.ndt.net/article/apcndt2013/papers/184.pdf > (Available: 28.12.2016).

[2] A.A. Carvalhoa, J.M.A. Rebello, L.V.S. Sagrilo, C.S. Camerini, I.V.J. Miranda, MFL signals and artificial neural networks applied to detection and classification of pipe weld defects, NDT&E Int. 39 (2006) 661–667.

[3] A.K. Hossam, A.G. Hossam, Review of pipeline integrity management practices, Int. J. Press. Vessels Pip. 87 (2010) 373–380.

[4] W. Shen, H. Songling, Z. Wei, W. Zheng, 3D modeling of circumferential SH guided waves in pipeline for axial cracking detection in ILI tools, Ultrasonics 56 (2015) 325–331.

[5] A.A. Mazraeh, W. Khaksar, F.B. Ismail, K.S.M. Sahari, Development of ultrasonic crack detection system on multi-diameter PIG Robots, Proc. Comput. Sci. 105 (2017) 282–288.

[6] M. Beller, Pipeline inspection utilizing ultrasound technology: on the issue of resolution, 2007, < http://ppsa-online.com/papers/2007-9-Beller.pdf > (Available: 25.07.2017).

[7] Y. Li, J. Wilson, G.Y. Tian, Experiment and simulation study of 3D magnetic field sensing for magnetic flux leakage defect characterization, NDT&E Int. 40 (2007) 179–184.

[8] R.C. Ireland, C.R. Torres, Finite element modelling of a circumferential magnetiser, Sens. Actuat. A 129 (2006) 197–202.

[9] D. Wu, Z. Liu, X. Wang, L. Su, Composite magnetic flux leakage detection method for pipelines using alternating magnetic field excitation, NDT and E Int. 91 (2017) 148–155.

[10] T. Jin, P. Que, T. Chen, Q. Zhang, Automatic data acquisition system for offshore oil pipeline magnetic flux leakage on-line inspection, J. Jpn. Pet. Inst. 48 (6) (2005) 380–385.

[11] J.-H. Park, H.-J. Kim, S.-J. Song, J.-W. Park, H.-R. Yoo, Y.-W. Rho, S.-H. Cho, D.-K. Kim, One-bed RFECT System for Inspection of Circumferential Cracks in 16 Inch Gas Pipeline, in: 10th International Conference on Ubiquitous Robots and Ambient Intelligence (URAI), 2013, pp. 59–62.

[12] A. Dubov, S. Kolokolnikov, Assessment of the material state of oil and gas pipelines based on the metal magnetic memory method, Weld. World 56 (3–4) (2012) 11–19.

[13] A. Dubov, A. Dubov, S. Kolokolnikov, Application of the metal magnetic memory method for detection of defects at the initial stage of their development for prevention of failures of power engineering welded steel structures and steam turbine parts, Weld World 58 (2014) 225–236.

[14] S.-J. Liu, M. Jiang, D.-A. He, Application of metal magnetic memory testing technology in pipeline defect, in: International Conference on Electronic, Control, Automation and Mechanical Engineering, 2017, pp. 233–236.

[15] K. Mandal, D. Dufour, T.W. Krause, D.L. Atherton, Investigations of magnetic flux leakage and magnetic Barkhausen noise signals from pipeline steel, J. Phys. D Appl. Phys. 30 (1997) 962–973.

[16] K. Mandal, A. Corey, M.E. Loukas, P. Weyman, J. Eichenberger, D.L. Atherton, The effects of defect depth and bending stress on magnetic Barkhausen noise and flux-leakage signals, J. Phys. D Appl. Phys. 30 (1997) 1976–1983.

[17] V.R. Skal's'kyi, E.P. Pochaps'kyi, B.P. Klym, M.O. Rudak, P.P. Velykyi, Application of the method of magnetoelastic acoustic emission for the analysis of the technical state of 19g steel after long-term operation in an oil pipeline, Materials Science, 52 (2016) 385–389.

[18] Z. Li, R. Jarvis, P.B. Nagy, S. Dixon, P. Cawley, Experimental and simulation methods to study the magnetic tomography method (MTM) for pipe defect detection, NDT and E Int. 92 (2017) 59–66.

[19] J.W. Wilson, G.Y. Tian, Pulsed electromagnetic methods for defect detection and characterization, NDT&E Int. 40 (2007) 275–283.

[20] M.M. Tehranchi, M. Ranjbaran, H. Eftekhari, Double core giant magneto-impedance sensors for the inspection of magnetic flux leakage from metal surface cracks, Sens. Actuat. A 170 (2011) 55–61.

[21] M.M. Tehranchi, S.M. Hamidi, H. Eftekhari, M. Karbaschi, M. Ranjbaran, The inspection of magnetic flux leakage from metal surface cracks by magneto-optical sensors, Sens. Actuat. A 172 (2011) 365–368.

[22] V. Babbar, L. Clapham, Residual magnetic flux leakage: a possible tool for studying pipeline defects, J. Nondestr. Eval. 22 (2003) 117–125.

[23] L. Xiang, L. Xunbo, C. Liang, Q. Guangxu, F. Peifu, H. Zuoying, Steel pipeline testing using magnetic flux leakage method, IEEE Int. Conf. Indus. Technol. (2008) 1–4.

[24] Y. Lijian, L. Gang, Z. Guoguang, G. Songwei, Sensor Development and Application on the oil-gas pipeline Magnetic Flux Leakage Detection, in: The Ninth International Conference on Electronic Measurement & Instruments (ICEMI'2009) 876–878.

[25] H.M. Kim, Y.W. Rho, H.R. Yoo, S.H. Cho, D.K. Kim, S.J. Koo, G.S. Park, A study on the measurement of axial cracks in the magnetic flux leakage NDT System, in: 8th IEEE International Conference on Automation Science and Engineering, 2012, pp. 624–629.

[26] H.M. Kim, H.R. Yoo, Y.W. Rho, G.S. Park, Detection method of cracks by using magnetic fields in underground pipeline, in: 10th International Conference on Ubiquitous Robots and Ambient Intelligence, 2013, pp. 734–737.

[27] A. Sophian, G.Y. Tian, S. Zairi, Pulsed magnetic flux leakage techniques for crack detection and characterisation, Sens. Actuat. A 125 (2006) 186–191.

[28] D. Zhou, M. Pan, Y. He, B. Du, Stress detection and measurement in ferromagnetic metals using pulse electromagnetic method with U-shaped sensor, Measurement 105 (2017) 136–145.

[29] KMZ51 Magnetic Field Sensor Product Specification Data Sheet, 1998.

[30] Application note, electronic compass design using KMZ51 and KMZ52, Thomas Stork.

[31] Y. Ege, A. Kakilli, H. Çıtak, M. Çoramık, Determination of buried magnetic material's geometric dimensions, Signal & Image Process.: An Int. J. (SIPIJ) 7 (5) (2016) 11–22.

[32] Y. Ege, A. Kakilli, H. Çıtak, O. Kalender, S. Nazlıbilek, M.G. Sensoy, New magnetic measurement system for determining metal covered mines by detecting magnetic anomaly using a sensor network, Indian J. Pure Appl. Phys. (IJPAP) 53 (2015) 199–211.